Advanced Pharmaceutical Bulletin

Accepted Manuscript (unedited)

The manuscript will undergo copyediting, typesetting, and review of the resulting proof before it is published in its final form.

Research Article

How to cite this article:
Abbaspour-Rvasjani S, Shahvalizadeh R, Safavi M, Afrashteh Nour M, Talebi M, Mohammadi M, Hamishehkar H. pH-Sensitive Folate-Targeted Liposomal Vitamin D Reprograms EZH2/STAT3 Axis and Induces Apoptosis, ROS, and Autophagy in MCF-7 Breast Cancer Cells. Advanced Pharmaceutical Bulletin, doi: 10.34172/apb.46791

pH-Sensitive Folate-Targeted Liposomal Vitamin D Reprograms EZH2/STAT3 Axis and Induces Apoptosis, ROS, and Autophagy in MCF-7 Breast Cancer Cells

Soheil Abbaspour-Rvasjani [a,b], Rahim Shahvalizadeh [b], Malahat Safavi [c], Mina Afrashteh Nour [d,b], Mahdi Talebi [e], Maryam Mohammadi [f], Hamed Hamishehkar [b,g]

a Student Research Committee, Department of Medical Nanotechnology, School of Medicine, Zanjan University of Medical Sciences, Zanjan, Iran
b Drug Applied Research Center, Tabriz University of Medical Sciences, Tabriz, Iran
c Department of Food Industry Science and Engineering, Faculty of Agriculture, University of Tabriz, Tabriz, Iran
d Department of Biochemistry and Clinical Laboratories, Faculty of Medicine, Tabriz University of Medical Sciences, Tabriz, Iran
e Department of Applied Cell Sciences, Faculty of Advanced Medical Sciences, Tabriz University of Medical Sciences, Tabriz, Iran
f Department of Food Science and Engineering, Faculty of Agriculture, University of Kurdistan, Sanandaj, Iran
g Research Center of New Material and Green Chemistry, Khazar University, 41 Mehseti Street, AZ1096, Baku, Azerbaijan

ARTICLE INFO

Keywords:
pH‑sensitive liposomes;
Vitamin D3;
Breast cancer;
Folate targeting;
MCF‑7 cells

Article History:
Submitted: November 20, 2025
Revised: May 25, 2026
Accepted: June 22, 2026
ePublished: July 01, 2026

ABSTRACT

Purpose: Vitamin D3 (Vit D3) possesses pleiotropic anticancer activity; however, its clinical application is limited by poor bioavailability and nonselective cellular uptake. This study aimed to develop folate (FA)-targeted, pH-sensitive liposomes for enhanced delivery of Vit D3 to breast cancer cells and to evaluate their effects on the VDR/EZH2/STAT3 signaling axis.

Methods: Vit D3-loaded pH-sensitive liposomes were formulated and characterized for particle size, zeta potential, encapsulation efficiency, stability, and pH-responsive release. Cellular uptake, cytotoxicity, clonogenicity, apoptosis, reactive oxygen species (ROS) generation, autophagy, cell-cycle distribution, RT-qPCR, and Western blotting were evaluated in MCF-7 cells.

Results: The optimized formulations exhibited nanoscale particle size, high encapsulation efficiency, physicochemical stability, and enhanced acidic pH-triggered release. FA-targeted liposomes significantly increased cellular uptake and cytotoxicity compared with free Vit D3 and non-targeted liposomes, with IC50 values of 15, 11, and 7.2 IU • mL-1, respectively. Vit D3-PEG/lipo-FA induced a 3.2-fold upregulation of VDR expression while suppressing EZH2 and STAT3 expression by 60% and 50%, respectively. In addition, treatment increased Caspase-3, LC3B, and NOX4 expression, promoted apoptosis and ROS generation, altered cell-cycle progression, and markedly reduced clonogenic survival. Western blot analysis confirmed these molecular alterations at the protein level.

Conclusion: FA-targeted pH-sensitive liposomal delivery significantly enhances the anticancer efficacy of Vit D3 in MCF-7 cells by modulating the VDR/EZH2/STAT3 axis and activating apoptosis-, autophagy-, and ROS-associated pathways, highlighting its potential as a targeted nanotherapeutic strategy for breast cancer treatment.

***Corresponding Author**
Hamed Hamishehkar, Email: hamishehkar.hamed@gmail.com, ORCID: 0000-0001-9905-0662

1. Introduction

Breast cancer remains one of the most prevalent and clinically challenging malignancies worldwide, accounting for substantial morbidity and mortality among women despite advances in detection and multimodal therapy.[1] Tumor heterogeneity, adaptive resistance mechanisms, and the complex interplay between oncogenic signaling and the tumor microenvironment continue to limit the efficacy of conventional chemotherapeutics and hormone therapies.[2] Consequently, there is an ongoing need for therapeutic strategies that combine selective tumor targeting with molecularly informed interventions to suppress key drivers of proliferation and survival while minimizing systemic toxicity.[3] Cholecalciferol (Vit D_3) and its active metabolites have emerged as biologically pleiotropic regulators with potential anticancer activity.[4] Beyond its classical role in calcium homeostasis, Vit D_3 modulates cell proliferation, differentiation, apoptosis, and immune responses through the Vit D receptor (VDR), a nuclear transcription factor expressed in many tissues, including breast epithelium and breast cancer cells.[5] Preclinical studies indicate that VDR activation can antagonize oncogenic signaling, induce cell‑cycle arrest, promote programmed cell death, and modulate epigenetic regulators.[6] Despite these promising activities, the clinical translation of Vit D_3 as an anticancer agent has been limited by its lipophilicity, poor aqueous solubility, rapid systemic metabolism, and the need for high local concentrations to achieve robust antitumor effects in vitro.[7,8] Delivering Vit D_3 selectively to cancer cells and enhancing its intracellular bioavailability, therefore, represents an attractive strategy to potentiate its anticancer potential.[9,10]

At the molecular level, two nodes of particular interest in breast cancer biology are EZH2 and STAT3. EZH2, the catalytic subunit of the Polycomb Repressive Complex 2 (PRC2), catalyzes trimethylation of histone H3 lysine 27 (H3K27me3) and acts as an epigenetic silencer of tumor suppressor genes; its overexpression is associated with aggressive phenotypes and poor prognosis in breast cancer.[11,12] STAT3 is a central transcriptional mediator of cytokine and growth factor signaling that drives proliferation, survival, invasion, and immune evasion; persistent STAT3 activation is frequently observed in breast tumors and contributes to therapy resistance.[13,14] Interactions between epigenetic regulators, such as EZH2, and signaling hubs, such as STAT3, create feed‑forward circuits that reinforce oncogenic programs.[15] Importantly, preclinical evidence suggests that modulation of VDR signaling can intersect with these pathways.[16] For example, Vit D_3 analogs have been reported to downregulate EZH2 expression and to inhibit STAT3 activation in some cancer models, highlighting the conceptual rationale for combining VDR activation with strategies that increase intracellular drug delivery.[17] Nanoparticle‑based drug delivery systems offer a solution to several of the pharmacological limitations of Vit D_3.[18] Liposomes, in particular, are biocompatible vesicles capable of encapsulating hydrophobic agents within their lipid bilayer, improving solubility, protecting cargo from premature metabolism, and providing opportunities for surface functionalization to achieve active targeting.[19] pH‑sensitive liposomes are engineered to be relatively stable at physiological pH (7.4) but destabilize in the mildly acidic environments characteristic of tumors or endolysosomal compartments (pH ~5.0–6.5), thereby promoting triggered release of the payload at the disease site or after endocytosis.[20]

In this study, we developed folate-targeted, pH-sensitive liposomes to deliver Vit D_3 selectively to MCF-7 breast cancer cells, addressing a gap where few studies jointly evaluate targeted, acid-triggered nanodelivery and downstream molecular effects. The study aimed to optimize Vit D_3-loaded liposomes for folate-mediated uptake and pH-triggered release, and to test whether enhanced intracellular delivery strengthens VDR signaling while suppressing EZH2/STAT3 and inducing apoptosis, autophagy, ROS generation, and cell-cycle changes. Formulation characterization and a panel of cellular assays were used to link liposome properties with biological

outcomes. The central hypothesis was that FA-targeted, pH-sensitive liposomes would deliver more Vit D_3 into MCF-7 cells than free drug or non-targeted liposomes, resulting in stronger VDR induction, greater EZH2/STAT3 suppression, and lower clonogenic survival.

2. Materials and methods

2.1. Materials

Methanol (≥99.9%, HPLC Grade), RPMI-1640-Medium, Tween 80®, Cholesteryl hemisuccinate (CHEMS), 4′,6-Diamidino-2-phenylindole dihydrochloride (DAPI), Anhydrous chloroform (≥99%), Isopropanol(≥99%), Vit D_3, Penicillin-Streptomycin (Pen-Strep), Trypsin-EDTA solution (0.25%), 3-(4,5-Dimethyl-2-thiazolyl)-2,5-diphenyl-2H-tetrazolium Bromide (MTT), Fetal Bovine Serum (FBS), dialysis cellulose membrane bags (MWCO 12,000 Da), Monodansylcadaverine (≥99.0%), 2′,7′-Dichlorofluorescin diacetate (DCFH-DA), RNase A solution (20 $mg.mL^{-1}$ in Tris buffer), Phosphate buffered saline tablets (PBS), TRI Reagent®, Triton X100, Dialysis tubing cellulose membrane (Mw = 14 KDa), Crystal violet solution (0.5%), Rhodamine B (≥95%), First Strand cDNA Synthesis Kit for RT-PCR (AMV), Propidium iodide (≥94.0%) and Annexin V-FITC/PI kit were all purchased from Sigma Aldrich Co. (Hamburg, Germany). 1,2-Dioleoyl-sn-glycero-3-PE (DOPE) and 1,2-distearoyl-sn-glycero-3-phosphoethanolamine-N-[folate(polyethylene glycol)-2000] (DSPE-PEG(2000) Folate) were obtained from Avanti Polar Lipids, Inc (Alabaster, AL).

2.2. Liposome formulation and preparation

PEGylated folic-acid–targeted Vit D_3 liposomes (Vit D_3-PEG/lipo-FA) were prepared using the thin-film hydration technique.[20] For untargeted PEGylated Vit D_3 liposomes (Vit D_3-PEG/lipo), DOPE, CHEMS, and DSPE-PEG2000 were combined at a molar ratio of 5.8:3.7:0.5 (total lipid mass = 10 mg). For the Vit D_3-PEG/lipo-FA formulation, DOPE, CHEMS, DSPE-PEG2000, and DSPE-PEG2000-Fol were mixed at a molar ratio of 5.8:3.7:0.45:0.05 (total lipid mass = 10 mg). Lipids were dissolved in chloroform, and 1000 IU of Vit D_3 and 1 mg of Tween 80® were added to each formulation. For blank formulation (PEG/lipo), the DOPE, CHEMS, and DSPE-PEG2000 lipid combination was used without Vit D_3. Finally, the solutions were transferred to a round-bottom flask, and the solvent was removed under reduced pressure to yield a dry lipid film. 100 µL of 0.1 M NaOH was applied to the film to ensure full ionization of CHEMS and to promote the formation of a lamellar structure, after which the film was hydrated with 300 mM ammonium sulfate at room temperature under vigorous stirring. The resulting liposomes were downsized by high-shear homogenization at 15,000 rpm and 65 °C for 20 minutes. External ammonium sulfate was removed using dialysis.

2.3. Physicochemical characterization

The mean liposome diameter was measured by dynamic light scattering (DLS) at 25 °C using a 90° scattering angle, and the zeta potential was measured by electrophoretic mobility under the same conditions. Size and zeta-potential determinations were performed in triplicate using a Nano ZS90 Zetasizer (Malvern Instruments, UK). Before analysis, samples were diluted tenfold with double-distilled, prefiltered water.

The encapsulation efficiency (EE%) and drug loading (DL%) of Vit D_3 were determined by HPLC (Knauer, Germany). Separation was carried out on a reversed-phase C18 column (250 × 4.6 mm, 5 µm) with UV detection at 265 nm, using a methanol:acetonitrile (20:80, v/v) mobile phase.

To isolate the liposomal fraction for analysis, 100 µL of Vit D3-PEG/lipo-FA suspension was mixed with 100 µL of acetone to precipitate the liposomal material, then centrifuged at 12,000 rpm for 15 min. The resulting sediment was air-dried at room temperature, dissolved in chloroform, and then diluted tenfold with the mobile phase before HPLC analysis. Calibration was performed using four Vit D_3 standard solutions (1–100 $IU.mL^{-1}$) prepared in

methanol:acetonitrile (80:20, v/v). The injection volume was 20 µL, and the mean retention time of Vit D_3 was 7.51 min. Linearity parameters, including r^2, slope, and intercept, were calculated. EE% and DL% were expressed as follows:

$$EE\% = \frac{Total\ amount\ of\ encapsulated\ Vit\ D_3}{Total\ vitamin\ D_3\ added} \times 100$$

$$DL\% = \frac{Total\ amount\ of\ entrapped\ Vit\ D_3}{Total\ amount\ of\ liposomes} \times 100$$

The morphology of the liposomes was examined by scanning electron microscopy (SEM; TESCAN; S8000; Czech Republic). Liposomal samples were diluted tenfold in double-distilled water, deposited onto aluminum foil, coated with gold, and imaged to visualize the surface structure.

2.4. Stability studies

The stability of Vit D_3–PEG/lipo-FA was evaluated by monitoring changes in average particle diameter, polydispersity index (PDI), and drug retention during storage. The formulations were kept in sealed vials at refrigerated temperature (4–8 °C) for 60 days. At predetermined intervals of 0, 15, 30, 45, and 60 days, samples were collected and examined for particle size and PDI using dynamic light scattering. Drug retention was assessed by calculating the percentage of encapsulated Vit D_3 remaining relative to the initial loading at each sampling time.[21]

2.5. *In vitro* release study

In vitro drug release was evaluated by dialysis using cellulose membrane bags against HEPES–saline buffer containing 1% Tween 80® at two pH values (5.5 and 7.4). Dialysis bags containing 500 µL of Vit D_3–PEG/lipo-FA were immersed in 25 mL of the release medium and agitated at 37 °C. At 1, 2, 3, 4, 8, 12, 24, and 48 h, 500 µL aliquots of the external medium were collected and immediately replaced with an equal volume of fresh buffer to maintain sink conditions. The amount of Vit D3 released from the collected samples was quantified by HPLC, and cumulative release was calculated, accounting for sample removal and replacement.[22]

2.6. Hemocompatibility

The hemocompatibility of Vit D_3–PEG/lipo-FA was determined using a hemolysis test, which measures the release of hemoglobin from red blood cells (RBCs) following exposure to nanoliposomes. Human whole blood was collected in sterile EDTA tubes and centrifuged at 1,500 rpm for 5 min. The plasma and buffy coat were discarded, and the RBC fraction was washed and resuspended in phosphate-buffered saline (PBS). Liposomal samples were prepared in PBS at final concentrations of 0 (negative control), 4, 5, 6, 7, 8, 9, and 10 mg/mL in a total volume of 1 mL. A 1% Triton X-100 solution was used as the positive control. The samples (Vit D_3–PEG/lipo-FA plus RBCs) were incubated at 37 °C for 1 h and then centrifuged at 1,500 rpm for 5 min. The absorbance of the resulting supernatant was recorded at 450 nm, and the percentage of hemolysis was calculated using the following equation:

$$Hemolysed\ blood\ (\%) = \frac{Absorbance(sample) - Absorbance(PBS)}{Absorbance(Ctrl\ Pos) - Absorbance(PBS)} \times 100$$

2.7. Cell culture and treatment

MCF-7 cells were obtained from the Pasteur Institute (Tehran, Iran) and cultured in RPMI-1640 medium supplemented with 10% FBS and 1% antibiotic solution. The cells were maintained at 37 °C in a humidified incubator with 5% CO_2. Subculturing was performed 24 and 48 h after seeding at an initial density of 4×10^4

cells.mL^{-1}. All experiments, including the MTT assay, flow cytometry, and fluorescence imaging, were initiated when the cultures reached approximately 70% confluence.

2.8. Cellular uptake assay

The internalization of targeted liposomes was investigated in MCF-7 cells, which show high folate receptor expression, and A549 cells, which exhibit low folate expression, using flow cytometry (Becton Dickinson, USA). Cells were seeded in 12-well plates at a density of 4×10^4 cells per well and allowed to attach overnight. Rhodamine B–labeled liposomal formulations (Rhodamine B-PEG/lipo and Rhodamine B-PEG/lipo-FA) were added at their respective IC_{50} concentrations. At 0, 1, 2, 4, 8, 12, and 24 h after treatment, the medium was removed, the cells were trypsinized, washed twice with PBS, and analyzed by flow cytometry. Mean fluorescence intensity was recorded, and the results were processed with FlowJo software.[1]

2.9. Cytotoxicity assay

Cell viability and proliferation were assessed using the MTT assay to compare the effects of Vit D_3, Vit D_3-PEG/lipo, and Vit D3-PEG/lipo-FA. Cells were seeded in 96-well plates at 1.2×10^4 cells per well and incubated overnight. To determine IC_{50} values, the cells were exposed to serial dilutions of Vit D_3, Vit D_3-PEG/lipo, and Vit D_3-PEG/lipo-FA for 48 h. After treatment, the medium was replaced with 100 µL of fresh medium and 50 µL of MTT solution (2 mg/mL in PBS), followed by incubation for 4 h at 37 °C. The resulting formazan crystals were dissolved in 100 µL DMSO, and absorbance was measured at 570 nm using a microplate reader (Sunrise™, Tecan, Switzerland).

2.10. Apoptosis assays

Apoptotic and necrotic cell populations were quantified using Annexin V/PI staining. MCF-7 cells were seeded in 6-well plates at a density of 4×10^5 cells per well and incubated overnight. The cells were then treated with each formulation at its IC_{50} concentration for 48 h. After treatment, the cells were collected by trypsinization, washed with PBS, and resuspended in 100 µL binding buffer. Staining with Annexin V/PI was carried out according to the manufacturer's protocol, and the samples were subsequently analyzed by flow cytometry. In addition, apoptotic and necrotic cells were qualitatively examined under a fluorescence microscope after DAPI/PI staining (Olympus BX50).[23,24]

2.11. Colony formation (clonogenic) assay

A clonogenic assay was used to evaluate long-term antiproliferative effects. MCF-7 cells were plated at 2×10^3 cells/well in 6-well plates and incubated for 48 h to allow attachment. Cells were then treated with EC_{10} concentrations of the formulations and maintained under standard culture conditions for two weeks. Colonies were fixed, stained with crystal violet, photographed, and counted using ImageJ software (NIH, Bethesda, MD).[25]

2.12. Cell morphology imaging

To assess morphological changes induced by our treatments, brightfield imaging was performed. MCF-7 cells were seeded on 20 mm coverslips at a density of 2×10^5 cells/well. After 48 h, cells were treated with formulations at their IC_{50} concentrations for an additional 48 h. Treated cells were washed twice with PBS, fixed in 4% formaldehyde for 4 h, washed again with PBS to remove residual fixative, and examined by brightfield microscopy.[26]

2.13. Cell cycle analysis

Cell cycle distribution was analyzed in MCF-7 cells seeded in 6-well plates at 4×10^5 cells per well. The cells were treated with Vit D_3, Vit D_3-PEG/lipo, and Vit D_3-PEG/lipo-FA at their IC_{50} concentrations for 48 h. Following trypsinization, the cells were fixed overnight in 70% ethanol. They were then treated overnight with

100 µg/mL RNase A, 50 µg/mL PI, and 0.1% Triton X-100, and finally analyzed by flow cytometry to determine DNA content and cell cycle phase distribution.[19]

2.14. Intracellular reactive oxygen species measurement

Intracellular reactive oxygen species (ROS) production was determined using DCFH-DA staining followed by flow cytometry. MCF-7 cells were seeded in 6-well plates at 4×10^5 cells per well and treated with the formulations at their 48-h IC_{50} concentrations. After 48 h, the cells were incubated with 10 µM DCFH-DA prepared in serum-free RPMI for 30 min at 37 °C. The cells were then washed twice with PBS, detached, and analyzed by flow cytometry. Green fluorescence was detected in the FL1-H channel.[27]

2.15. Autophagy assays

Monodansylcadaverine (MDC) staining was employed to detect autophagic vacuoles and visualize autophagy activation in MCF-7 cells. Cells were seeded onto 12-mm coverslips at 2×10^5 cells/well and incubated for 48 h. Cultures were then treated with formulations at their IC_{50} concentrations for 48 h, washed twice with PBS, and stained with 0.05 mmol. L^{-1} MDC for 10 min at 37 °C. After three washes with PBS to remove excess dye, cells were examined by fluorescence microscopy.[23]

2.16. Gene expression analysis (RT‑qPCR)

Gene expression levels were measured by quantitative real-time PCR. MCF-7 cells were seeded at a density of 3×10^4 cells per well and incubated overnight to allow attachment. The cells were then treated with the formulations at their 48-h IC_{50} concentrations and incubated for an additional 48 h.

Total RNA was extracted using TRI Reagent®. Briefly, 1.0 mL of TRI Reagent® was added to each well, and the lysate was allowed to stand for 20 min. The mixture was then centrifuged at 4 °C for 5 min, and the supernatant was transferred to a new tube. Next, 200 µL of chloroform was added, the sample was mixed gently, and incubated at −20 °C for 20 min. After centrifugation at 12,000 rpm for 15 min at 4–8 °C, the aqueous phase was recovered, and RNA was precipitated by adding 500 µL isopropanol followed by 10 min of incubation. The RNA pellet was washed with isopropanol, air-dried, and dissolved in 20 µL RNase-free water. RNA concentration and purity were determined using a NanoDrop 2000 spectrophotometer (Thermo Fisher Scientific).

Complementary DNA (cDNA) was synthesized using the QuantiTect Reverse Transcription kit (Qiagen, Hilden, Germany). Quantitative PCR was performed with Power SYBR® Green PCR Master Mix (Applied Biosystems, Foster City, CA), using β-actin as the internal control. Relative expression of the target genes (VDR, EZH2, STAT3, CASP3, BCL2, LC3B, and NOX4) and β-actin was calculated by the $2^{-\Delta\Delta CT}$ method.[28] Primer sequences are listed in Table 1

Table 1: Primer sequences.

Gene	Forward	Reverse
β-actin	5'- CACCATTGGCAATGAGCGGTTC -3'	5'- AGGTCTTTGCGGATGTCCACGT -3'
VDR	5'-TCTCCAATCTGGATCTGAGTGAA-3'	5′-GGATGCTGTAACTGACCAGGT-3′
EZH2	5'- AGGACGGCTCCTCTAACCAT -3'	5'- CTTGGTGTTGCACTGTGCTT -3'

STAT3	5'- CAGCGAGAGCAGCAAAGAAG -3'	5'- GGAATGTCGGGGTAGAGGTAG -3'
CASP3	5′-GGAAGCGAATCAATGGACTCTGG-3′	5′-GCATCGAACATTGTACCAGACC-3′
BCL2	5'- ATCGCCCTGTGGATGACTGAGT -3'	5'- GCCAGGAGAAATCAAACAGAGGC -3'
MAP1LC3B	5'- CGGAGAAGACCTTCAAGCAG -3'	5'- CTGGGAGGCATAGACCATGT -3'
NOX4	5′-TAGATACCCACCCTCCC-3′	5′-GACTTATGACCGAAATGA-3′

2.17. Western blotting Assay

Western blot analysis was conducted to confirm the RT-PCR results. Following MCF-7 cells treatment with PEG/lipo, Vit D_3, Vit D_3-PEG/lipo, and Vit D_3-PEG/lipo-FA, the cells were rinsed with ice-cold phosphate-buffered saline and lysed on ice for 30 min using a protein extraction buffer composed of 25 mM HEPES, 1% Triton X-100, 2 mM EDTA, 0.1 M NaCl, 25 mM NaF, 1 mM sodium orthovanadate, and a protease inhibitor cocktail (Roche). The lysates were then centrifuged at 12,000 × g for 20 min at 4 °C, and the resulting supernatants were collected. Protein concentrations were measured by the bicinchoninic acid (BCA) method. Equal amounts of protein from each sample were combined with loading buffer, denatured, separated by 12.5% SDS-PAGE, and transferred to PVDF membranes. To reduce nonspecific interactions, the membranes were blocked with 5% skim milk in Tris-buffered saline containing 0.1% Tween-20 (TBST), and then incubated overnight at 4 °C with the relevant primary antibodies. After washing, the membranes were exposed to horseradish peroxidase (HRP)-linked secondary antibodies for 1 h at room temperature. Protein bands were detected using an enhanced chemiluminescence (ECL) system (Bio-Rad). Band density was assessed by ImageJ software (version 1.54) and normalized against the corresponding loading control.[29]

2.18. Statistical analysis

All experiments were conducted in triplicate using independent biological replicates. Statistical processing was performed with GraphPad Prism software, version 10.6.1 (GraphPad Software, San Diego, CA). Depending on the experimental design, the data were analyzed using either an unpaired Student's t-test or two-way analysis of variance (two-way ANOVA). When comparisons involved more than two groups, Tukey's post hoc test was used to identify significant differences. A p value of less than 0.05 was considered to indicate statistical significance.

3. Results

3.1. Liposome formulation and physicochemical characterization

All formulations displayed a narrow size distribution and negative surface charge. As shown in Fig. 1, number-weighted mean diameters were 30.26 ± 10.14 nm for PEG/lipo, 61.28 ± 2.95 nm for Vit D_3–PEG/lipo, and 83.54 ± 7.18 nm for Vit D_3–PEG/lipo-FA. Corresponding zeta potentials were −16.3 ± 5.83 mV, −20.5 ± 7.66 mV, and −21.0 ± 7.10 mV, respectively. Electron microscopy (SEM) revealed predominantly spherical particles and supported the size measurements (Fig. 1). Encapsulation efficiency (EE) of Vit D_3 was very high for both drug-loaded formulations: 97.3 ± 3.06% for Vit D_3–PEG/lipo and 98.2 ± 1.13% for Vit D_3–PEG/lipo-FA. Drug loading (DL, sometimes reported as loading capacity, LC) values were 9.73 ± 0.30% and 9.82 ± 0.11% for Vit D_3–PEG/lipo and Vit D_3–PEG/lipo-FA, respectively.

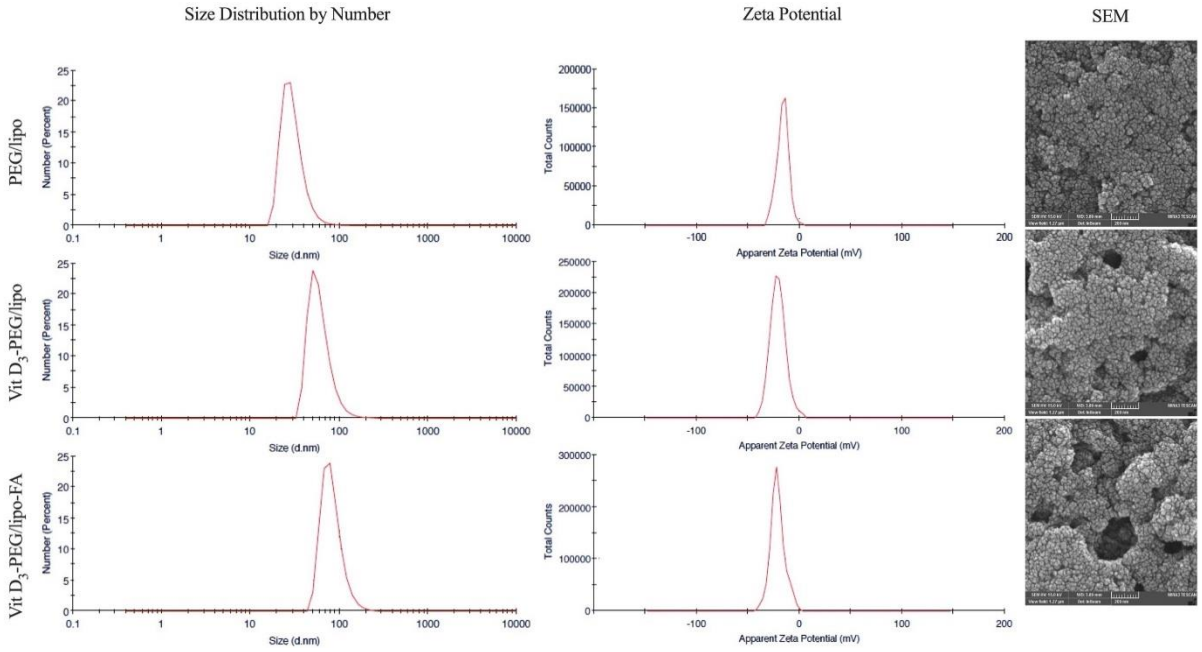

Figure 1. Physicochemical and morphological characterization of liposomal formulations. The left panels present the particle size distributions based on number for each formulation. The middle panels show the zeta potential distributions. The right panels display representative scanning electron microscopy (SEM) micrographs. The results indicate a uniform particle size distribution below 100 nm and a gradual change in surface properties after folic acid (FA) conjugation. Representative SEM images are shown, with scale bars indicated in each panel.

3.2. Formulation stability, *in vitro* release and hemocompatibility

Stability testing of Vit D_3–PEG/lipo-FA over 60 days under refrigerated storage (4–8 °C) showed no substantial changes in mean hydrodynamic diameter or PDI across sampling points (Fig. 2a). Leakage of Vit D_3 was measured every 15 days (Fig. 2b): cumulative release was 2.48 ± 0.52% at day 15, 4.24 ± 0.93% at day 30, 6.16 ± 1.31% at day 45, and 8.12 ± 1.12% at day 60. Statistical analysis indicated significant differences between day 0 and day 60, and between day 15 and day 60 (Fig. 2b).

pH-dependent release of Vit D_3–PEG/lipo-FA was assessed at pH 5.5 and pH 7.4 (Fig. 2c). Release was similar at both pH values for the first hour, after which the formulation exhibited a time- and pH-dependent release profile. From 2 to 12 hours the drug release was significantly greater at pH 5.5 than at pH 7.4 ($p < 0.05$), consistent with destabilization of the nanosystem under acidic conditions and supporting potential selective release in acidic tumor microenvironments.

Hemocompatibility testing (Fig. 2d) showed minimal red-blood-cell hemolysis across the concentration range tested (0.5–10 mg/mL). Even at the highest concentration (10 mg/mL), PEG/lipo-FA induced only 3.12% hemolysis, which is negligible compared with the positive control (1% Triton X-100, defined as 100% hemolysis).

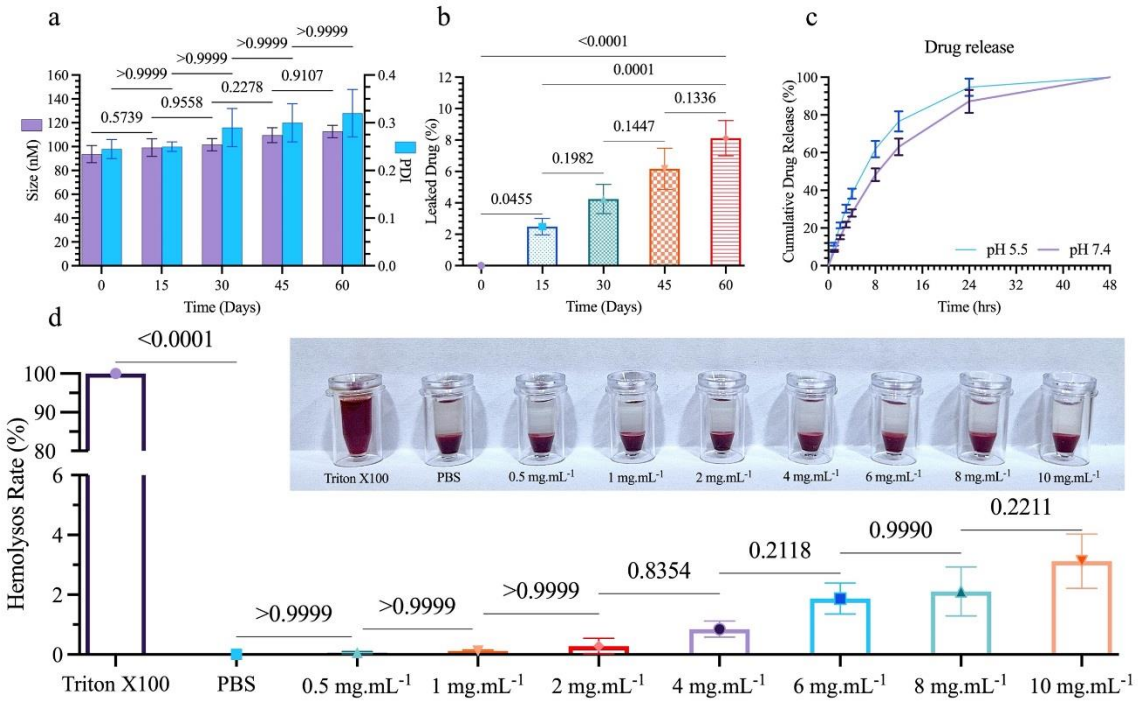

Figure 2. Stability, leakage, release and hemocompatibility. (a) Changes in hydrodynamic diameter and PDI of the formulations during 60 days of refrigerated storage. (b) Cumulative leakage of Vit D_3 from Vit D_3–PEG/lipo-FA over 60 days. (c) Cumulative in vitro drug release profiles at pH 5.5 and pH 7.4. (d) Hemolysis (%) induced by PEG/lipo-FA on human red blood cells. Data are reported as mean ± SD (n = 3). Statistical comparisons are indicated on the panels.

3.3. Cell Uptake

Cellular internalization of Rhodamine-B–labeled non-targeted and FA-targeted liposomes was compared in MCF-7 (high folate receptor expression) and A549 (lower folate receptor expression) cells (Fig. 3). Uptake by MCF-7 cells increased with time (Fig. 3a), and FA-decorated liposomes showed markedly higher internalization than non-targeted liposomes ($p < 0.0001$). In A549 cells both targeted and non-targeted formulations were taken up (Fig. 3b), but no statistically significant difference was observed between them ($p > 0.05$). These results indicate that folate decoration enhances uptake in folate-receptor–overexpressing cells, consistent with receptor-mediated endocytosis.

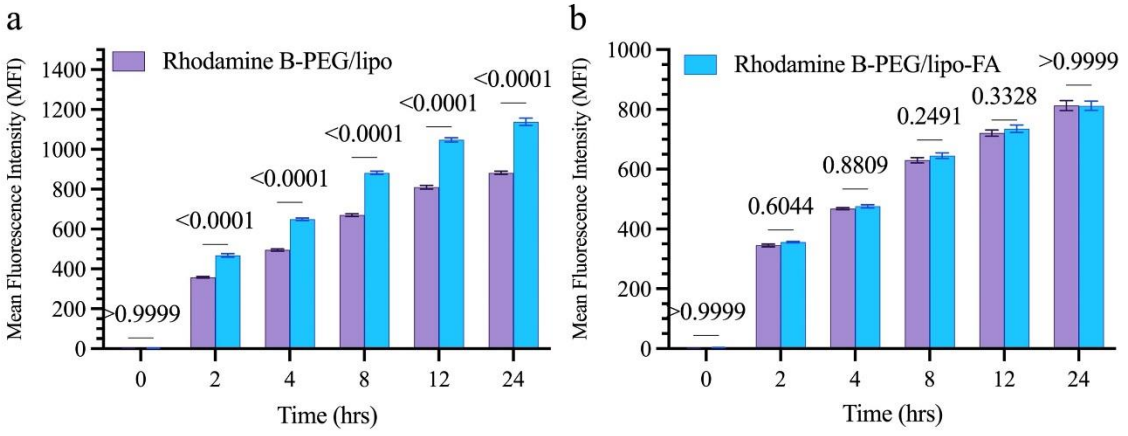

Figure 3. Cellular uptake measured by flow cytometry. Mean fluorescence intensity (MFI) of Rhodamine-B–labeled liposomes with and without FA decoration in MCF-7 and A549 cells at the indicated time points. Data are presented as mean ± SD (n = 3). Statistical comparisons are indicated on the panels.

3.4. Cytotoxicity.

The cytotoxic effects after 48 h exposure are summarized in Fig. 4. The MTT assay yielded IC_{50} values of approximately 15 IU·mL⁻¹ for free Vit D_3, ~11 IU·mL⁻¹ for the encapsulated (non-targeted) formulation, and ~7.2 IU·mL⁻¹ for the folate-targeted liposomal formulation. Encapsulation and subsequent folate targeting therefore produced progressive increases in cytotoxic potency against MCF-7 cells.

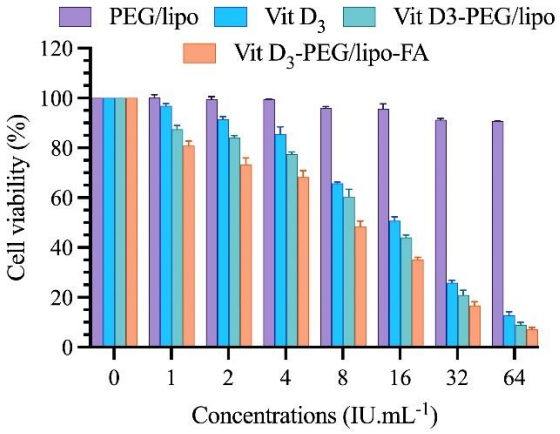

Figure 4. 48-hour cytotoxicity. Dose–response effects of PEG/lipo, Vit D_3, Vit D_3–PEG/lipo and Vit D_3–PEG/lipo-FA on MCF-7 cell viability (assessed by MTT) after 48 h. Data are presented as mean ± SD (n = 3).

3.5. Apoptosis, necrosis and DNA fragmentation

Annexin V/PI analysis and nuclear staining were used to distinguish viable, apoptotic and necrotic populations (Fig. 5). Treatment with free Vit D_3 produced 14.9% necrosis, 2.38% early apoptosis and 22.4% late apoptosis. Encapsulation into liposomes significantly reduced necrosis to 3.05% ($p = 0.0002$), produced a nonsignificant increase in early apoptosis to 4.66% ($p = 0.7922$), and significantly increased late apoptosis to 30.9% ($p = 0.0090$) relative to free Vit D_3. Addition of FA targeting produced a nonsignificant increase in necrosis (6.49%; $p = 0.5292$ versus Vit D_3–PEG/lipo), a significant rise in early apoptosis to 22.2% ($p = 0.0001$ versus Vit D_3–PEG/lipo), and a significant decrease in late apoptosis to 23.9% ($p = 0.0395$ versus Vit D_3–PEG/lipo). DAPI/PI micrographs (Fig. 5b) corroborated the flow-cytometry results by showing nuclear condensation and fragmentation consistent with apoptotic death.

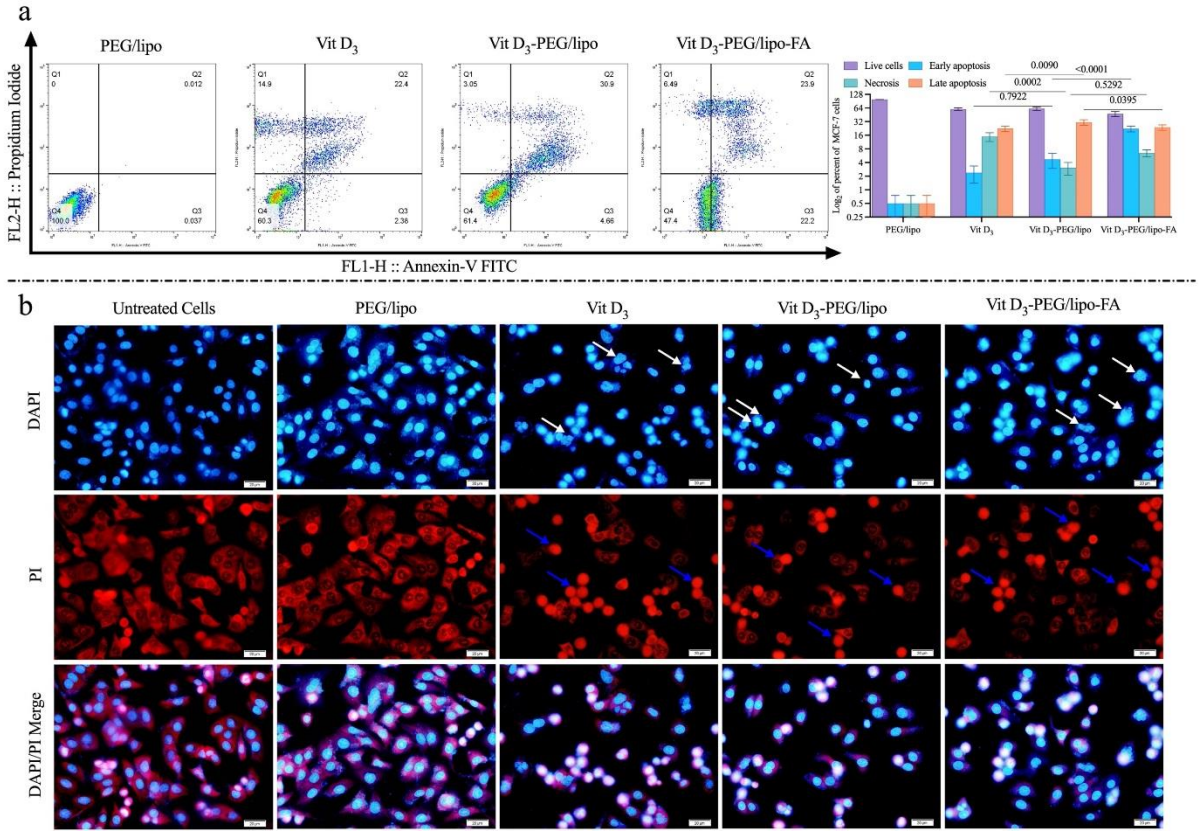

Figure 5. Apoptosis quantification and nuclear morphology. (a) Annexin V/PI flow-cytometric analysis showing percentages of viable, early apoptotic, late apoptotic and necrotic MCF-7 cells following treatment. (b) Representative DAPI/PI micrographs of treated cells (×400 magnification) highlighting nuclear condensation and fragmentation. Quantitative apoptosis results are reported as mean ± SD (n = 3). Scale bars are shown in the images. White arrows indicate apoptotic nuclei; blue arrows indicate necrotic nuclei.

3.6. Colony formation, cell morphology and autophagy activation

Clonogenic assays assessed long-term antiproliferative effects (Fig. 6a). Compared with the empty vehicle (PEG/lipo), free Vit D_3 reduced colony number by approximately 54% ($p < 0.0001$). Encapsulation into liposomes produced an additional significant reduction in colony formation relative to free Vit D_3 ($p = 0.0014$). FA targeting produced the strongest inhibition, yielding approximately 90% suppression of colony formation compared with the non-targeted formulation ($p = 0.0010$).

Morphological analysis (Fig. 6b) showed that cells treated with free Vit D_3 exhibited both necrotic and apoptotic features. Encapsulation reduced the proportion of necrotic cells while increasing apoptotic morphology. Cells treated with Vit D_3–PEG/lipo-FA displayed the greatest degree of cytoplasmic granulation and morphological alteration among groups.

Autophagy activation was evaluated qualitatively by MDC staining (Fig. 6c). Control cells (PEG/lipo) exhibited diffuse MDC fluorescence, whereas cells treated with Vit D_3–PEG/lipo and Vit D_3–PEG/lipo-FA showed a punctate MDC staining pattern indicative of autophagic vacuole formation. The FA-targeted formulation induced more pronounced puncta than non-targeted liposomes or free Vit D_3, suggesting stronger induction of autophagy.

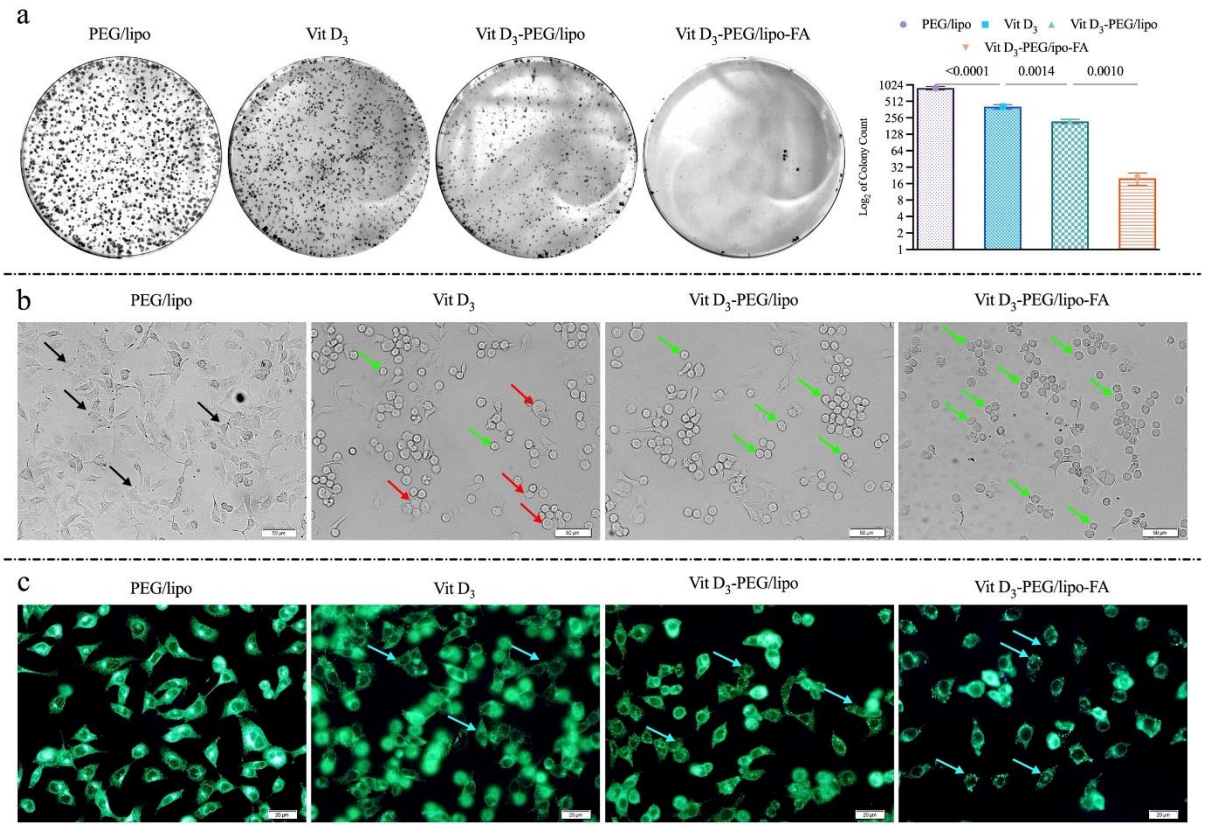

Figure 6. Long-term proliferation, morphology and autophagy. (a) Representative images and quantification of colony-formation assays showing the antiproliferative effect of each formulation after two weeks. (b) Brightfield images showing treatment-induced changes in MCF-7 cell morphology (200× magnification). (c) Fluorescence micrographs showing MDC-stained autophagic vacuoles in MCF-7 cells (400× magnification). Colony counts are reported as mean ± SD (n = 3). Scale bars are shown. Black arrows indicate morphologically normal cells; red arrows indicate necrotic cells; green arrows indicate apoptotic cells; turquoise (cyan) arrows indicate autophagic vacuoles.

3.7. ROS induction

Intracellular ROS levels were measured by DCFH-DA staining and flow cytometry (Fig. 7). Treatment with free Vit D_3 significantly increased ROS levels by ~51 % relative to PEG/lipo controls ($p = 0.0376$). Encapsulation significantly augmented ROS production relative to free Vit D_3 (~111% increase; $p = 0.0001$). FA targeting further and significantly increased ROS compared with the non-targeted liposomal formulation (~27% increase; $p < 0.0003$). These data indicate that encapsulation and folate targeting amplify Vit D_3-induced oxidative stress in MCF-7 cells.

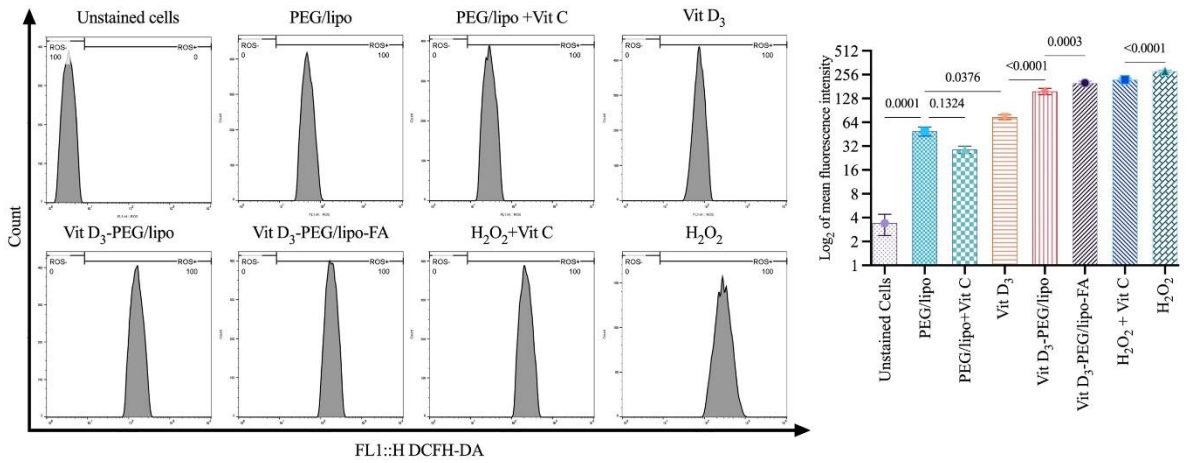

Figure 7. Oxidative stress induction. Flow-cytometric analysis of intracellular reactive oxygen species (ROS) in MCF-7 cells after treatment with the indicated formulations; results are expressed as mean fluorescence intensity (MFI). Data are presented as mean ± SD (n = 3).

3.8. Folate-targeted liposomal Vit D3 alters cell-cycle distribution and modulates the VDR/EZH2/STAT3 axis, apoptosis, autophagy, and oxidative stress

Cell-cycle distribution and relative gene and protein expression were assessed after 48 h treatment with PEG/lipo, free Vit D_3, Vit D_3-PEG/lipo, and Vit D_3-PEG/lipo-FA (Fig. 8).

Treatment with Vit D_3-PEG/lipo-FA caused a marked accumulation of cells in the Sub-G1 phase, indicating apoptotic DNA fragmentation (Fig. 8a). The Sub-G1 fraction increased from 1.0 ± 0.54% in the PEG/lipo group to 23.0 ± 3.12% in the Vit D_3-PEG/lipo-FA group ($p < 0.0001$). In parallel, the S-phase population decreased significantly from 30.0 ± 6.64% to 12.0 ± 4.67% ($p < 0.0001$), and the G2/M fraction declined from 14.0 ± 2.87% to 5.0 ± 1.76% ($p = 0.0670$). No significant difference was observed in the G0/G1 fraction between the Vit D_3-PEG/lipo-FA and PEG/lipo groups (60.0 ± 4.58% vs. 55.0 ± 5.87%; $p = 0.4896$). These findings indicate that folate-targeted liposomal Vit D_3 induces cell-cycle arrest-associated cytotoxicity and promotes apoptotic cell death in MCF-7 cells.

At the molecular level, RT-qPCR showed that Vit D_3-PEG/lipo-FA significantly increased VDR expression by 3.2 ± 0.48-fold compared with PEG/lipo controls ($p = 0.0001$). At the same time, EZH2 and STAT3 were significantly downregulated to 0.40 ± 0.06 ($p = 0.0001$) and 0.50 ± 0.08 ($p = 0.0001$), respectively (Fig. 8b). In addition, Caspase-3 was upregulated to 2.5 ± 0.38-fold ($p = 0.0118$), whereas Bcl-2 was reduced to 0.50 ± 0.08 ($p = 0.0001$). The autophagy marker LC3B increased to 2.0 ± 0.30 ($p = 0.0001$), and NOX4 increased to 1.8 ± 0.27 ($p = 0.0001$). Western blot analysis confirmed these changes at the protein level (Fig. 8c). Vit D_3-PEG/lipo-FA increased VDR expression and reduced EZH2 and STAT3 protein levels, while also elevating cleaved Caspase-3, LC3B, and NOX4 and decreasing Bcl-2. Together, these data show that folate-targeted liposomal Vit D_3 reprograms the VDR/EZH2/STAT3 axis and promotes apoptosis, autophagy, ROS generation, and cell-cycle disruption in MCF-7 breast cancer cells.

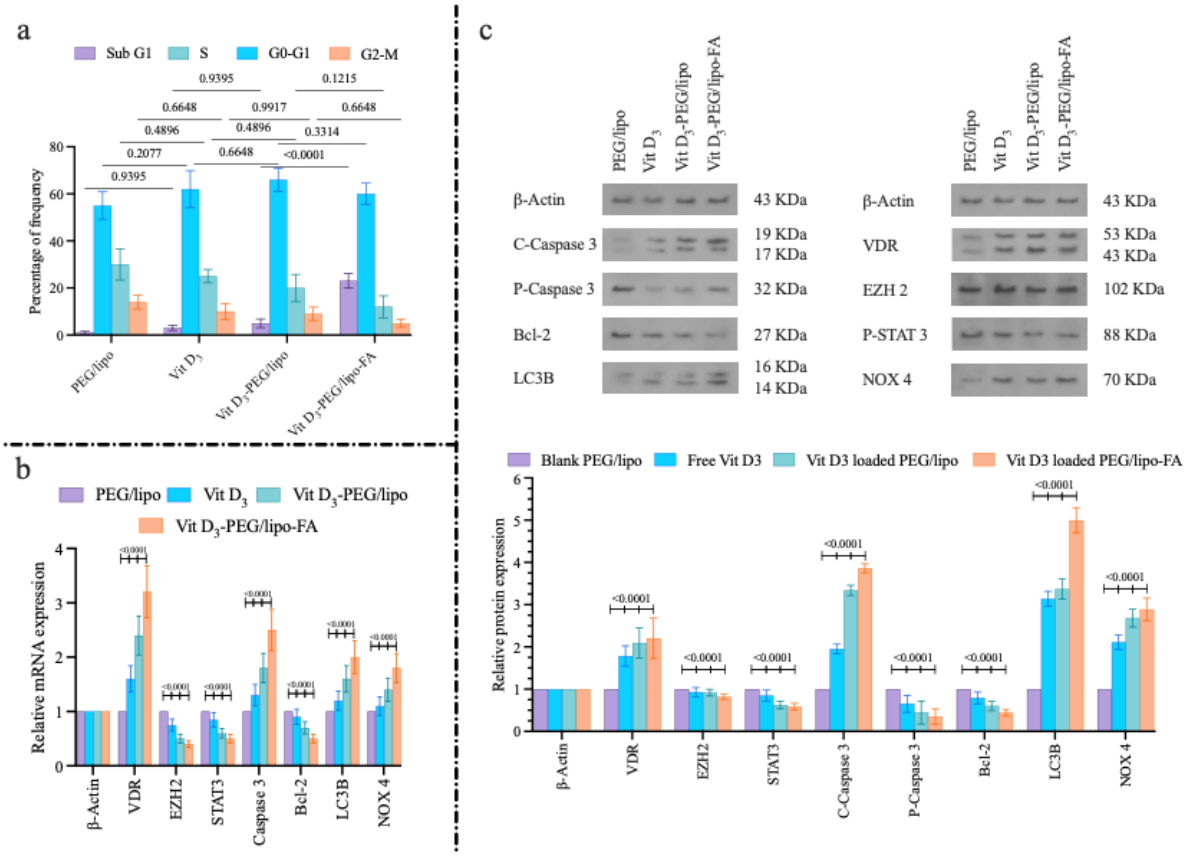

Figure 8. Cell-cycle analysis and molecular responses of MCF-7 cells following treatment with Vit D_3 formulations. (a) Cell-cycle distribution measured by flow cytometry after 48 h treatment. (b) Relative mRNA expression of VDR, EZH2, STAT3, CASP3, BCL2, LC3B, and NOX4 determined by RT-qPCR. (c) Relative protein expression of the same markers was determined by Western blotting. Data are mean ± SD (n = 3); statistical comparisons are shown in the figure.

4. Discussion

This study demonstrates that Vit D_3–PEG/lipo-FA produces a multi-modal antitumor response in MCF-7 breast cancer cells through improved physicochemical properties, receptor-mediated uptake, pH-responsive release, and coordinated modulation of apoptosis, oxidative stress and autophagy pathways. The combined set of in vitro data supports a mechanism in which targeted delivery both increases intracellular drug delivery and biases cell fate toward programmed cell death rather than uncontrolled necrosis.

From a formulation perspective, the liposomes exhibit attributes desirable for tumor-directed delivery. The number-weighted mean diameters (≈61 nm for non-targeted drug-loaded liposomes and ≈84 nm for FA-targeted liposomes) fall within the size range favorable for enhanced tumor accumulation via the enhanced permeability and retention (EPR) effect while remaining small enough for efficient cellular uptake.[3] The negative zeta potentials observed are consistent with colloidal stability and with the very high encapsulation efficiencies (>97%) and appreciable drug loading (~9.7–9.8%).[30] Refrigerated storage for 60 days produced minimal changes in hydrodynamic size and PDI and only modest cumulative leakage (<9% at day 60), indicating acceptable short-term stability. Hemocompatibility testing also returned reassuring results: negligible hemolysis even at high particle concentrations suggests a low risk of direct erythrocyte damage in systemic exposure scenarios.[31] Collectively, these physicochemical properties provide a sound delivery vehicle for further biological interrogation.

Biologically, FA decoration markedly improved functional delivery in folate receptor overexpressing MCF-7 cells: rhodamine-labeled FA-liposomes were internalized more rapidly and to a greater extent than non-targeted liposomes, and this enhanced uptake translated into increased cytotoxic potency (IC_{50} reduced from ~15 IU·mL^{-1}

for free drug to ~7.2 IU·mL^{-1} for Vit D_3–PEG/lipo-FA).[22] The pH-sensitive release profile similar release at neutral and acidic pH during the first hour followed by significantly greater release at pH 5.5 further supports a tumor- or endosome-selective release mechanism, where acidic compartments amplify payload liberation after receptor-mediated endocytosis.[20]

At the cellular response level, targeted liposomal Vit D_3 shifted the mode of cell death toward apoptosis and away from necrosis. Encapsulation alone reduced necrosis dramatically (from ~15% to ~3%), and FA targeting increased early apoptotic fractions while maintaining elevated late apoptosis levels an outcome that is typically more favorable therapeutically because it limits pro-inflammatory necrotic responses and promotes controlled cell clearance.[32-34] The strong increase in the Sub-G1 population and the pronounced inhibition of clonogenic growth (≈90% reduction with FA targeting vs non-targeted liposomes) together indicate both acute cytotoxicity and durable suppression of proliferative potential.[25]

Molecular profiling was consistent with these phenotypic effects. Vit D_3–PEG/lipo-FA increased VDR expression while suppressing EZH2 and STAT3, suggesting reprogramming of a pro-survival signaling network. In parallel, Caspase-3 and LC3B were upregulated, Bcl-2 was downregulated, and NOX4 expression and DCFH-DA fluorescence increased, indicating activation of apoptotic signaling, autophagy, and oxidative stress. Importantly, autophagy in cancer can be context dependent: it may serve as a cytoprotective adaptation that helps stressed cells survive, or it may contribute directly to cell death when excessively activated or dysregulated. In the present study, the concomitant rise in LC3B, MDC-positive puncta, apoptosis, and loss of clonogenic survival suggests that autophagy is associated with the overall cytotoxic response, although its exact functional role here remains to be clarified.[35-39]

5. Conclusion

Folate-targeted PEGylated liposomal delivery of vit D_3 exhibited favorable physicochemical properties sub-100 nm size range, high encapsulation efficiency, and short-term colloidal stability combined with excellent hemocompatibility. In folate-receptor–positive MCF-7 cells, FA decoration markedly enhanced uptake and produced pH-responsive payload release, leading to substantially increased cytotoxicity versus free Vit D_3 and non-targeted liposomes. Mechanistic findings show coordinated modulation of the VDR/EZH2/STAT3 axis, increased ROS generation, caspase-associated apoptosis, and induction of autophagic markers, together yielding both immediate apoptotic responses and durable suppression of clonogenic growth. These data support a model in which targeted liposomal Vit D_3 redirects pro-survival signaling toward oxidative-stress–driven apoptosis with concurrent autophagy activation. Overall, Vit D_3–PEG/lipo-FA is a promising delivery platform to potentiate the antitumor activity of Vit D_3 and warrants protein-level validation, mechanistic perturbation studies, and in vivo efficacy, pharmacokinetic, and safety evaluations to advance toward clinical translation.

Study limitation

This study has several limitations. First, the findings were obtained in a single breast cancer cell line (MCF-7), which limits generalizability across breast cancer subtypes; therefore, validation in triple-negative and HER2-positive models, as well as in non-cancerous breast cells, is needed to better define tumor selectivity and safety. Second, although key molecular changes were confirmed by RT-qPCR and Western blotting, the causal roles of ROS and autophagy in Vit D_3-induced cell death were not directly tested using pharmacological inhibitors or genetic knockdown approaches. Third, the work was restricted to an in vitro setting, and therefore, the in vivo efficacy, biodistribution, pharmacokinetics, systemic toxicity, and antitumor activity of the formulation remain unknown. Fourth, stability and hemocompatibility were evaluated only under limited laboratory conditions and over a 60-day refrigerated period; long-term stability and behavior under physiological stress conditions were not

assessed. Finally, scale-up feasibility and translational performance have not yet been examined. These issues should be addressed in future preclinical studies.

Ethical Approval

In reporting our findings, we adhere to the highest standards of publication ethics. This includes transparent disclosure of any potential conflicts of interest and proper acknowledgment of prior work and collaborative contributions. Our primary concern is the safety and welfare of researchers, study participants, and the environment. To ensure this, all laboratory personnel receive thorough training in safe laboratory practices. Strict safety measures are followed when working with cell cultures, hazardous materials, and laboratory equipment.

Authors' Contribution

Conceptualization: Hamed Hamishehkar and Soheil Abbaspour-Rvasjani.

Data curation: Hamed Hamishehkar and Soheil Abbaspour-Rvasjani.

Formal analysis: Soheil Abbaspour-Rvasjani.

Investigation: Soheil Abbaspour-Rvasjani, Rahim Shahvalizadeh, Malahat Safavi, and Mina Afrashteh Nour.

Methodology: Soheil Abbaspour-Rvasjani, Rahim Shahvalizadeh, Malahat Safavi, and Mina Afrashteh Nour.

Project administration: Hamed Hamishehkar.

Resources: Hamed Hamishehkar and Malahat Safavi.

Software: Soheil Abbaspour-Rvasjani.

Supervision: Hamed Hamishehkar, and Maryam Mohammadi.

Validation: Maryam Mohammadi, Soheil Abbaspour-Rvasjani and Hamed Hamishehkar

Writing–original draft: Soheil Abbaspour-Rvasjani.

Writing–review & editing: Soheil Abbaspour-Rvasjani.

Funding

This project was financially supported by the Drug Applied Research Center, Tabriz University of Medical Sciences, Tabriz, Iran (Grant number: 62529).

Conflict of interest

The authors of the manuscript entitled "pH-Sensitive Folate-Targeted Liposomal Vitamin D_3 Reprograms EZH2/STAT3 Axis and Induces Apoptosis, ROS, and Autophagy in MCF-7 Breast Cancer Cells" declare no conflicts of interest about the submitted manuscript.

References

1. Mahoutforoush A, Asadollahi L, Hamishehkar H, Abbaspour-Ravasjani S, Solouk A, Haghbin Nazarpak MH. Targeted Delivery of Pennyroyal via Methotrexate Functionalized PEGylated Nanostructured Lipid Carriers into Breast Cancer Cells; A Multiple Pathways Apoptosis Activator. *Adv Pharm Bull* 2023;13(4):747–60. doi: 10.34172/apb.2023.077

2. Wu P, Gao W, Su M, Nice EC, Zhang W, Lin J, et al. Adaptive Mechanisms of Tumor Therapy Resistance Driven by Tumor Microenvironment. *Front Cell Dev Biol* 2021;9. doi: 10.3389/fcell.2021.641469

3. Zeinali M, Abbaspour-Ravasjani S, Ghorbani M, Babazadeh A, Soltanfam T, Santos AC, et al. Nanovehicles for co-delivery of anticancer agents. *Drug Discov Today* 2020;25(8):1416–30. doi: 10.1016/j.drudis.2020.06.027

4. Loo YS, Yusoh NA, Zahid NI, Madheswaran T, Ikeno S, Nurdin A, et al. Vitamin D3-PEGylated hexosomes for gemcitabine and thymoquinone co-delivery: Unraveling the physicochemical characteristics, biocompatibility, and cytotoxicity against breast cancer cells. *J Drug Deliv Sci Technol* 2025;114. doi: 10.1016/j.jddst.2025.107445

5. Simioni YR, Perez NS, Barbosa LRS, Perez AP, Schilrreff P, Romero EL, et al. Enhancing the anti-psoriatic activity of vitamin D3 employing nanostructured archaeolipid carriers. *J Drug Deliv Sci Technol* 2022;73. doi: 10.1016/j.jddst.2022.103455

6. Muralidhar S, Filia A, Nsengimana J, Poźniak J, O'Shea SJ, Diaz JM, et al. Vitamin D–VDR signaling inhibits Wnt/b-catenin–mediated melanoma progression and promotes antitumor immunity. *Cancer Res* 2019;79(23):5986–98. doi: 10.1158/0008-5472.CAN-18-3927

7. Chiang KC, Chen TC. The anti-cancer actions of vitamin D. *Anticancer Agents Med Chem* 2013;13(1):126–39. doi: 10.2174/187152013804487443

8. Gupta R, Behera C, Paudwal G, Rawat N, Baldi A, Gupta PN. Recent Advances in Formulation Strategies for Efficient Delivery of Vitamin D. *AAPS PharmSciTech* 2019;20(1). doi: 10.1208/s12249-018-1231-9

9. Krishnan AV, Feldman D. Mechanisms of the anti-cancer and anti-inflammatory actions of vitamin D. *Annu Rev Pharmacol Toxicol* 2011;51:311–36. doi: 10.1146/annurev-pharmtox-010510-100611

10. Hussain M, Xu J, Ahmad I, Hussain K, Qayum A, Xiaoqin L, et al. Efficacy of Nano-Based Strategies on the Safe Delivery and Bioavailability of Vitamin D: Review. *Food Rev Int* 2024;40(6):1581–99. doi: 10.1080/87559129.2023.2225591

11. Zhao Y, Hu Z, Li J, Hu T. EZH2 exacerbates breast cancer by methylating and activating STAT3 directly. *J Cancer* 2021;12(17):5220–30. doi: 10.7150/jca.50675

12. Park SH, Fong KW, Mong E, Martin MC, Schiltz GE, Yu J. Going beyond Polycomb: EZH2 functions in prostate cancer. *Oncogene* 2021;40(39):5788–98. doi: 10.1038/s41388-021-01982-4

13. Yu H, Pardoll D, Jove R. STATs in cancer inflammation and immunity: A leading role for STAT3. *Nat Rev Cancer* 2009;9(11):798–809. doi: 10.1038/nrc2734

14. Singh S, Gomez HJ, Thakkar S, Singh SP, Parihar AS. Overcoming Acquired Drug Resistance to Cancer Therapies through Targeted STAT3 Inhibition. *Int J Mol Sci* 2023;24(5). doi: 10.3390/ijms24054722

15. Samad MA, Ahmad I, Hasan A, Alhashmi MH, Ayub A, Al-Abbasi FA, et al. STAT3 Signaling Pathway in Health and Disease. *MedComm* 2025;6(4). doi: 10.1002/mco2.70152

16. Deeb KK, Trump DL, Johnson CS. Vitamin D signalling pathways in cancer: Potential for anticancer therapeutics. *Nat Rev Cancer* 2007;7(9):684–700. doi: 10.1038/nrc2196

17. Zhang Q, Jia R, Chen M, Wang J, Huang F, Shi M, et al. Antagonizing EZH2 combined with vitamin D3 exerts a synergistic role in anti-fibrosis through bidirectional effects on hepatocytes and hepatic stellate cells. *J Gastroenterol Hepatol* 2023;38(3):441–50. doi: 10.1111/jgh.16126

18. Mohammadi M, Pezeshki A, Mesgari-Abbasi MM, Ghanbarzadeh B, Hamishehkar H. Vitamin D3-loaded nanostructured lipid carriers as a potential approach for fortifying food beverages; in vitro and in vivo evaluation. *Adv Pharm Bull* 2017;7(1):61–71. doi: 10.15171/apb.2017.008

19. Abbaspour-Ravasjani S, Zeinali M, Asadollahi L, Safavi M, Mahoutforoush A, Talebi M, et al. Hyaluronic Acid-Functionalized Liposomes for Co-delivery of 5-Fluorouracil and Cannabidiol Against Colorectal Cancer. *Adv Pharm Bull* 2025;15(4):819–35. doi: 10.34172/apb.025.43401

20. Nunes SS, Miranda SEM, de Oliveira-Silva J, Fernandes RS, de Alcantara Lemos J, Ferreira C, et al. pH-responsive and folate-coated liposomes encapsulating irinotecan as an alternative to improve efficacy of colorectal cancer treatment. *Biomed Pharmacother* 2021;144:112317. doi: 10.1016/j.biopha.2021.112317

21. Gaballu FA, Abbaspour-Ravasjani S, Mansoori B, Yekta R, Hamishehkar H, Mohammadi A, et al. Comparative of in-vitro evaluation between erlotinib loaded nanostructured lipid carriers and liposomes against A549 lung cancer cell line. *Iran J Pharm Res* 2019;18(3):1168–79. doi: 10.22037/ijpr.2019.1100775

22. Abedi Gaballu F, Cho WCS, Dehghan G, Zarebkohan A, Baradaran B, Mansoori B, et al. Silencing of hmga2 by sirna loaded methotrexate functionalized polyamidoamine dendrimer for human breast cancer cell therapy. *Genes (Basel)* 2021;12(7). doi: 10.3390/genes12071102

23. Asadollahi L, Abbaspour-Ravasjani S, Kim KA, Maghsoodi M, Hamishehkar H, Kosari‐Nasab M, et al. Rice (Oryza sativa) Stem Cells as a Novel Promising Active Ingredient with Anti-Proliferative Effects for Potential Skin Cancer Prevention and Skin Whitening Activity. *Foods* 2024;13(17). doi: 10.3390/foods13172803

24. Sepasi T, Ghadiri T, Ebrahimi-Kalan A, Bani F, Talebi M, Rahbarghazi R, et al. CDX-modified chitosan nanoparticles remarkably reduce therapeutic dose of fingolimod in the EAE model of mice. *Int J Pharm* 2023;636. doi: 10.1016/j.ijpharm.2023.122815

25. Mansoori B, Mohammadi A, Abedi-Gaballu F, Abbaspour S, Ghasabi M, Yekta R, et al. Hyaluronic acid-decorated liposomal nanoparticles for targeted delivery of 5-fluorouracil into HT-29 colorectal cancer cells. *J Cell Physiol* 2020;235(10):6817–30. doi: 10.1002/jcp.29576

26. Mahoutforoush A, Solouk A, Hamishehkar H, Haghbin Nazarpak M, Abbaspour-Ravasjani S. Novel decorated nanostructured lipid carrier for simultaneous active targeting of three anti-cancer agents. *Life Sci* 2021;279. doi: 10.1016/j.lfs.2021.119576

27. Zeinali M, Abbaspour-Ravasjani S, Soltanfam T, Paiva-Santos AC, Babaei H, Veiga F, et al. Prevention of UV-induced skin cancer in mice by gamma oryzanol-loaded nanoethosomes. *Life Sci* 2021;283. doi: 10.1016/j.lfs.2021.119759

28. Asghariazar V, Vahidian F, Karimi A, Abbaspour-Ravasjani S, Mansoori B, Safarzadeh E. The Role of Oleuropein, Derived from Olives, in Human Skin Fibroblast Cells: Investigating the Underlying Molecular Mechanisms of Cytotoxicity and Antioxidant and Anti-Inflammatory Activities. *Int J Clin Pract* 2024;2024. doi: 10.1155/2024/8827501

29. Dianat-Moghadam H, Abbasspour-Ravasjani S, Hamishehkar H, Rahbarghazi R, Nouri M. LXR inhibitor SR9243-loaded immunoliposomes modulate lipid metabolism and stemness in colorectal cancer cells. *Med Oncol* 2023;40(6). doi: 10.1007/s12032-023-02027-4

30. Midekessa G, Godakumara K, Ord J, Viil J, Lättekivi F, Dissanayake K, et al. Zeta Potential of Extracellular Vesicles: Toward Understanding the Attributes that Determine Colloidal Stability. *ACS Omega* 2020;5(27):16701–10. doi: 10.1021/acsomega.0c01582

31. Shanmugam PST, Sampath T, Jagadeeswaran I, Krithaksha V, Bhalerao VP, Thamizharasan S. Hemocompatibility. Elsevier; 2023. p. 91–125.

32. Gao W, Meng T, Shi N, Zhuang H, Yang Z, Qi X. Targeting and Microenvironment-Responsive Lipid Nanocarrier for the Enhancement of Tumor Cell Recognition and Therapeutic Efficiency. *Adv Healthc Mater* 2015;4(5):748–59. doi: 10.1002/adhm.201400675

33. Wang TS, Coppens I, Saorin A, Brady NR, Hamacher-Brady A. Endolysosomal Targeting of Mitochondria Is Integral to BAX-Mediated Mitochondrial Permeabilization during Apoptosis Signaling. *Dev Cell* 2020;53(6):627–45.e7. doi: 10.1016/j.devcel.2020.05.014

34. Reddy JA, Low PS. Folate-mediated targeting of therapeutic and imaging agents to cancers. *Crit Rev Ther Drug Carrier Syst* 1998;15(6):587–627. doi: 10.1615/critrevtherdrugcarriersyst.v15.i6.20

35. Nurminen V, Seuter S, Carlberg C. Primary Vitamin D target genes of human monocytes. *Front Physiol* 2019;10(MAR). doi: 10.3389/fphys.2019.00194

36. Cucick ACC, Laiño JE, de Moreno de LeBlanc A, Herkenhoff ME, Suzuki JY, Franco BDGM, et al. Impact of folate bio-enriched fermented beverage on vitamin D receptor and folate transporters expression in the colon: Insights from in vitro and in vivo studies. *Food Biosci* 2025;65. doi: 10.1016/j.fbio.2025.106106
37. Tang M, Gong M, Liu X, Zhang T, Liu Z, Song D. Recent update on the development of EZH2 inhibitors and degraders for cancer therapy. *Eur J Med Chem* 2025;299. doi: 10.1016/j.ejmech.2025.118106
38. Verma S, Goyal N, Goyal S, Kaur P, Gupta S. EZH2 Dysregulation and Its Oncogenic Role in Human Cancers. *Cancers (Basel)* 2025;17(19). doi: 10.3390/cancers17193111
39. Zhang B, Fan J, Zhang X, Shen W, Cao Z, Yang P, et al. Targeting asparagine and autophagy for pulmonary adenocarcinoma therapy. *Appl Microbiol Biotechnol* 2016;100(21):9145–61. doi: 10.1007/s00253-016-7640-3